POLITECNICO DI TORINO
Repository ISTITUZIONALE

Understanding powder transport mechanisms in directed energy deposition via design of experiments

Original
Understanding powder transport mechanisms in directed energy deposition via design of experiments / Pilagatti, A.N., Atzeni, E., Salmi, A., Iuliano, L.. - 57:(2025), pp. 128-135. (17th Italian Manufacturing Association Conference, AITeM 2025 ita 2025) [10.21741/9781644903735-15].

Availability:
This version is available at: 11583/3008567 since: 2026-03-11T09:42:53Z

Publisher:
Association of American Publishers

Published
DOI:10.21741/9781644903735-15

Terms of use:

This article is made available under terms and conditions as specified in the corresponding bibliographic description in the repository

Publisher copyright

(Article begins on next page)

19 November 2026

Materials Research Proceedings 57 (2025) 128-135 https://doi.org/10.21741/9781644903735-15

Understanding powder transport mechanisms in directed energy deposition via design of experiments

Adriano Nicola PILAGATTI[1,a *], Eleonora ATZENI[1,b], Alessandro SALMI[1,c] and Luca IULIANO[1,d]

[1]Department of Management and Production Engineering (DIGEP), Politecnico di Torino, Corso Duca degli Abruzzi 24, 10129 Torino, Italy

[a]adriano.pilagatti@polito.it, [b]eleonora.atzeni@polito.it, [c]alessandro.salmi@polito.it, [d]luca.iuliano@polito.it

Keywords: Additive Manufacturing; Laser Processes; Design of Experiment; Manufacturing Systems

Abstract. Laser beam powder metal directed energy deposition (DED-LB/Powder) is a metal additive manufacturing (AM) technique that can build, repair, and remanufacture metal components. The objective of this study is to investigate the behaviour of the powder supply system, based on a rotating disk powder metering and pneumatic conveying. The powder mass flow rate was related to different levels of carrier gas flow rate and perforated disc rotation. A sensor acquisition system was designed to measure and acquire the boundary conditions (BCs) exterior to the powder feeder system, in order to identify possible external noise. Based on the data analysis, it was possible to identify different feeding conditions as the input parameters were varied and how the responses were affected by them.

Introduction

Directed Energy Deposition (DED) is an additive manufacturing (AM) category that uses focused thermal energy to fuse feedstock material as it is deposited along a programmed path. Depending on the energy source employed, DED can be distinguished into laser-based (LB), electric arc (Arc), and electron beam (EB) processes. The feedstock material can be supplied as either a continuous wire or a powder stream. When a laser beam is used as the thermal source for fusing powdered material, the process is specifically referred to as DED-LB/Powder, in accordance with ISO/ASTM 52900:2021(E) [1].

A key aspect in determining the impact of DED-LB/Powder processes on part quality is the correct tuning of the powder mass flow rate ($\dot{m}_{\mathrm{powder}}$). Precise control of $\dot{m}_{\mathrm{powder}}$ is essential for maintaining process stability, achieving uniform material deposition, and optimizing mechanical properties [2]. The structured powder handling mechanism used by the DED-LB/Powder systems basically consists of three interrelated phases: powder metering, powder conveyance, and powder delivery. The first phase is the metering, either in mass or volume, of the amount of powder to be fed into the melt pool from the reservoir. Powder metering can be achieved by a number of methods including aspirating/dispensing, screw/auger, feeder wheel, and electrostatic. In the second phase the powder is conveyed from the metering device to the nozzle. This is usually accomplished by an inert carrier gas flow. Other conveyance methods include mechanical conveyance, as well as vibration-assisted and gravity-driven conveyance. The third phase, accomplished via a powder delivery nozzle, converges the powder stream into a single focal spot. The pipe system connecting the feeding system to the deposition head [2-5] and the nozzle configuration define the transport mechanism. Despite the clear distinction made here between powder metering, conveyance, and delivery, it should be emphasised that these phases are frequently interconnected. Collectively, these phases determine the efficiency and reliability of the powder deposition process [6].

Content from this work may be used under the terms of the Creative Commons Attribution 3.0 license. Any further distribution of this work must maintain attribution to the author(s) and the title of the work, journal citation and DOI. Published under license by Materials Research Forum LLC.

Materials Research Proceedings 57 (2025) 128-135 https://doi.org/10.21741/9781644903735-15

The effectiveness of powder transport and deposition is influenced by the interplay between powder feeding parameters. Understanding these interactions is essential for improving process stability and optimizing deposition efficiency. Several research studies have optimized feeding parameters in the literature. Among them, Oh *et al.* [7], explored gas flow rate between 4 L min^{-1} and 6 L min^{-1} for AISI 316L and reported that increasing the carrier gas flow rate reduces the powder flow rate, thereby lowering the height of the deposited material. However, excessive powder flow can exceed the desired dimensions, highlighting the need for optimization alongside other process parameters. Regarding powder transport studies, Iams *et al.* [8] examined how variations in particle size affect $\dot{m}_{powder}$ in DED processes. Their findings demonstrated that even a slight increase in particle size results in higher flow resistance. This increase in resistance, attributable to larger and heavier particles, leads to a corresponding decrease in the powder velocity. Simoneau *et al.* [9] emphasized that a defined powder flow rate (2.1 g min^{-1},) and a controlled particle size distribution contribute to improved powder fluidity within the DED feeding system. This suggests that powder flow rate is a key factor influencing process consistency and reproducibility of mechanical properties. Whiting *et al.* [10] used an Optomec powder feeder to monitor the metallic powder mass flow in a DED process with an acoustic emission sensor. They calibrated the system for flow levels ranging from 4 rpm to 8 rpm using AISI 316L powder and established a correlation between the acoustic signal and the actual mass flow rate. This innovative method accurately detects minor flow fluctuations and, with the integration of waveguides, enables more precise and reliable in situ process control, enhancing overall system performance.

The present study aims to characterize the powder mass flow rate, $\dot{m}_{powder,}$ in a DED-LB/Powder system by evaluating the effects of powder feeding parameters. Boundary conditions are monitored as covariates to identify potential noise. To achieve this, the study employs analysis of covariance (ANCOVA) within the framework of the design of experiments (DoE) methodology. The objective is to improve predictive accuracy and enhance process stability by examining the interactions among these factors. The response surface methodology (RSM) approach is used to develop a response surface model. This model enables the identification of both stable combinations of parameters and the onset of undesired effects such as fluctuations in powder flow, which are correlated with the powder feeding mechanisms.

Material and Methods

The experimental setup consisted of a Laserdyne 430 DED system (Prima Additive, Italy) and an Optomec CS 150 powder feeder (Albuquerque, NM, USA), depicted in Fig. 1. The gravity-type powder feeder employs a perforated disk metering system, rotating around a horizontal axis, to regulate powder flow through an orifice on a coupled fixed disk. Pressurised gas is employed to enable suction and conveyance of powders.

Disk rotation speed (ω) and carrier gas flow rate ($\dot{V}_{cg}$) serve as the primary control factors for the powder mass flow rate. The powder feeder is connected to the deposition head by a flexible polymer pipeline with an internal diameter of 6.35 mm and a total length of 2.4 m. The powder feeder has upper limits of 24 rpm for ω and 10 L min^{-1} for $\dot{V}_{cg}$. The deposition head features four distinct nozzles with a nominal diameter of 1 mm each. These nozzles converge the powder stream at an 8 mm standoff distance, ensuring optimal delivery and uniform distribution of the powder material.

Feedstock Material. The feedstock material is gas-atomized MetcoAdd AISI 316L stainless steel powder (Oerlikon, Switzerland) with a particle size distribution ranging from 45 µm to 106 µm (D10 = 54 µm, D50 = 79 µm, D90 = 110 µm), a powder density of 7.896(0.005) g cm^3, and a Carr's compressibility index of 8.3 %, confirming excellent powder flow characteristics [11].

Materials Research Proceedings 57 (2025) 128-135 https://doi.org/10.21741/9781644903735-15



Fig. 1: Optomec CS 150 powder feeder system metering chamber.

Boundary Conditions Monitoring System. Uncontrollable factors, namely chamber temperature (T) and absolute humidity (Ha), were measured as BCs to assess, if present, their impact on $\dot{m}_{powder}$. A custom ESP32-based monitoring system was developed to track BCs. The system employs a Bosch BME280 sensor housed in an IP55-protected enclosure within the build chamber, ensuring exposure only to the measurement environment. Data were recorded at 100 Hz and processed using a simple moving average filter to eliminate transient fluctuations.

Experimental Design. Argon was used as carrier gas. A design comprising four levels for $\dot{V}_{Ar}$, and six levels for ω, equally spaced, was employed to investigate the effects of varying factors on the resulting $\dot{m}_{powder}$ at the nozzles. Based on knowledge from previous experiments, ω varied from 2 rpm to 22 rpm, avoiding the upper limit of 24 rpm due to frequent mechanical issues. A range for $\dot{V}_{Ar}$, from 2 L min^{-1} to 8 L min^{-1}, was explored, with the objective of expanding the typical range reported in the literature. A two-step approach was used to determine the sample size [12]. First, a priori calculations were conducted using G*Power 3.1.9.4, a software tool developed by the Heinrich Heine University of Düsseldorf (Düsseldorf, Germany), resulting in a minimum sample size of 69 [13]. To ensure adequate statistical power and simplify design replications, a sample size of 72 was selected corresponding to a factorial design with 6 levels of ω and 4 levels of $\dot{V}_{Ar}$, and 3 replications (as depicted in Fig. 2). A post hoc type II error analysis confirmed that the selected sample size was sufficient, achieving 99 % power for $\dot{V}_{Ar}$, 97 % for ω and 68 % for the interaction term (Table 1). These results validate the robustness of the experimental design and its ability to detect significant effects.

Table 1: Post hoc computed type II error for the experiment conducted with 72 trials.

Factor	*df*	Critical *F*	Power [%]
$\dot{V}_{Ar}$	3	2.8	99
ω	5	2.4	97
$\omega \cdot \dot{V}_{Ar}$	15	1.9	68

Materials Research Proceedings 57 (2025) 128-135 https://doi.org/10.21741/9781644903735-15

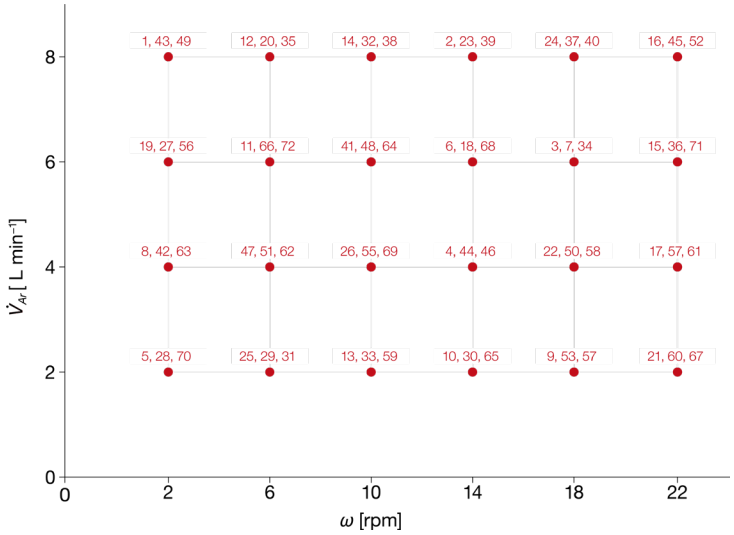


Fig. 2: General Full Factorial design with levels and run orders.

Powder Flow Rate Measurement. The $\dot{m}_{powder}$ was measured using a dual-bottle collection method designed to differentiate between transient and steady-state powder flow (see Fig. 3). The first bottle (with the blue funnel) collected the powder flow during the transient phases (30 s), corresponding to the activation and deactivation of the powder stream. The second bottle (with the black funnel) exclusively captured powder during the steady-state phase (120 s), ensuring a more accurate measurement of the delivered powder in stable condition. The entire procedure was programmed using G-code. Following each trial, the powder from the steady-state bottle was weighed using a high-precision ANJ-NM/ABS -N balance by KERN (Gottlieb, Germany). Finally, the $\dot{m}_{powder}$ was determined as the ratio of the collected mass to the flow time. After measurement, the powder from both bottles was carefully removed, sieved, and recycled. The bottles were then repositioned on the machine table to ensure consistency across measurements.



Fig. 3: Experiment setup for powder mass flow rate.

Materials Research Proceedings 57 (2025) 128-135 https://doi.org/10.21741/9781644903735-15

Table 2. Analysis of covariance (R^2(adj)=99 %).

Source	*df*	Contribution [%]	Adj *SS*	Adj *MS*	*F*	*p*-value [%]
Model	25	99.37	3153.64	126.145	291.78	<0.1
Covariates	2	5.93	0.76	0.379	0.88	42.3
***T* [°C]**	1	2.66	0.45	0.455	1.05	31.0
***H*$_a$ [g m^{-3}]**	1	4.54	0.53	0.532	1.23	27.3
Linear	8	79.97	2504.51	313.063	724.13	<0.1
***ω* [rpm]**	5	47.45	981.03	196.205	453.83	<0.1
$\dot{V}_{Ar}$[L min^{-1}]	3	32.52	865.53	288.508	667.34	<0.1
2-Way Interactions						
ω·$\dot{V}_{Ar}$ [rpm L min^{-1}]	15	13.47	427.41	28.494	65.91	<0.1
Error	46	0.63	19.89	0.432		
Total	71	100				

Results and discussion

Attention was given to avoiding systematic errors throughout the experiment. Thus, the experimental campaign was conducted on a single day by a single operator. To minimize errors due to the gas flow regulation system, the $\dot{V}_{Ar}$ was initially maximized and then cautiously reduced to the correct rate during the transient phase of each test. All trials were carried out with the same argon upstream flow rate (10 L min^{-1}) of the feeder system. The test order was randomized.

During the experiments covariate ranges were detected, which were between 25.2 °C and 29.5 °C for the temperature and 10.3 g m^{-3} and 12.4 g m^{-3} for absolute humidity. The analysis is conducted using MINITAB® 20.1.3 software (Gaithersburg, MD, USA). Data results are evaluated by ANCOVA (see Table 2) to identify if noise factors are active in the process, and neither covariate appears to influence $\dot{m}_{powder}$. Consequently, covariates are not taken into consideration for the next steps of the work. However, covariate acquisition could be helpful over the long term, and data are stored for future studies. The outliers analysis reveals issues with the 14 rpm (ω) level and low $\dot{V}_{Ar}$ values (2 L min^{-1} and 4 L min^{-1}); specifically, these issues are observed in the trials with Run Order 30 and 65 (14 rpm and 2 L min^{-1}) and Run Order 4 (14 rpm and 4 L min^{-1}). Data analysis reveals that linear terms contribute most to total Adj *SS*, with a greater contribution for the ω. Furthermore, the main effects and the interaction are significant for the significance level chosen, as confirmed by their *p*-value.

The R^2(adj) of 99 % indicates that the resulting model properly explains the variability of the data. Fig. 4(a) displays the plot of the main effects. As expected, as the ω factor increases, the response $\dot{m}_{powder}$ mean increases too. This is attributable to the greater quantity of powder entering the flow in a given time, consequent to an increase in disk rotation speed. However, at speeds exceeding 18 rpm, a decline in the $\dot{m}_{powder}$ mean response was observed. Conversely, the $\dot{V}_{Ar}$ factor demonstrated a counterintuitive tendency, in fact as the $\dot{V}_{Ar}$ increases, the $\dot{m}_{powder}$ decreases.

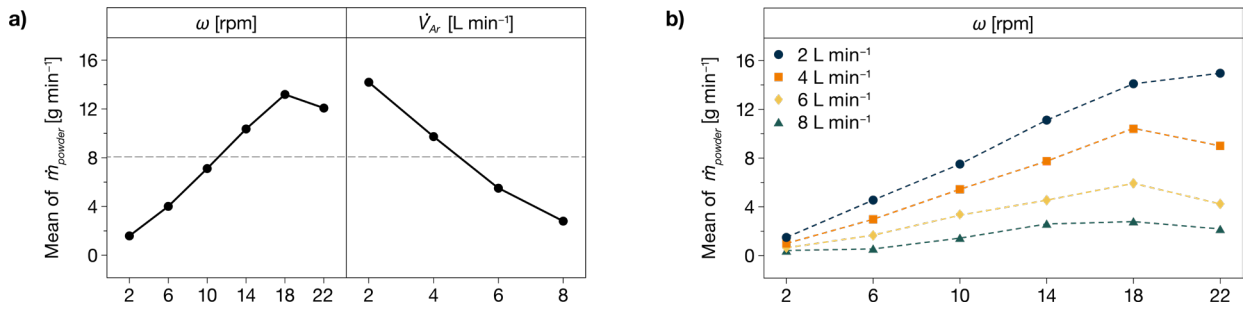


Fig. 4: (a) Main Effects plot and (b) Interaction plot for $\dot{m}_{powder}$ [g min^{-1}].

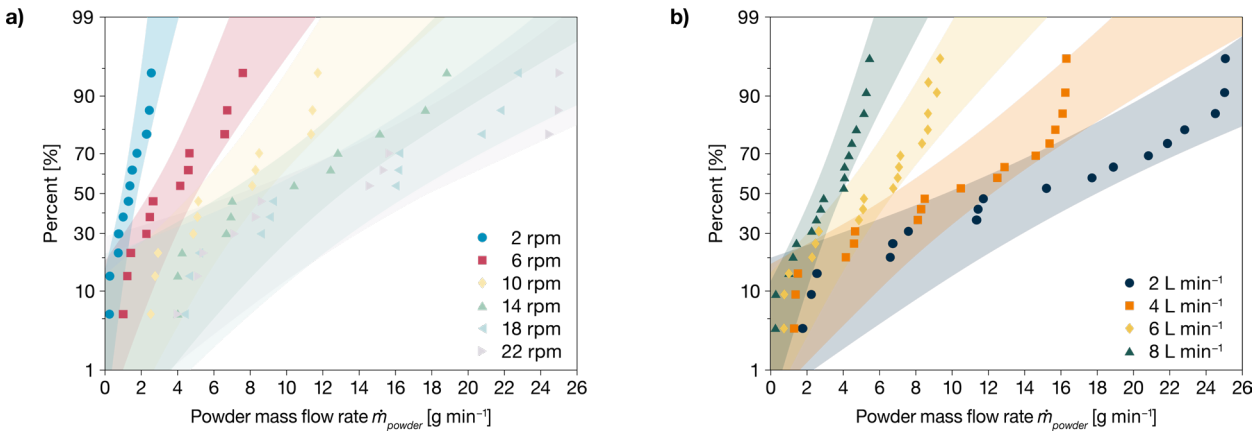


Fig. 5: Factorial main effect probability plot, Johnson's method, (a) versus ω and (b) versus $\dot{V}_{Ar}$ with the corresponding 95 % confidence intervals bands.

The interaction plot in Fig. 4(b) details that this trend is consistently observed across all levels of the ω factor, although it becomes more pronounced as both ω and $\dot{V}_{\mathrm{Ar}}$ increase. Furthermore, it is evident that the as $\dot{V}_{\mathrm{Ar}}$ increases, the inversion of the $\dot{m}_{powder}$ mean trend occurs at a lower ω. The normal probability plot (NPP) using Johnson's method (Fig. 5) highlights differences in means and variability across factor levels. However, despite absolute changes in standard deviation, the coefficient of variation remains stable, indicating that variability is primarily driven by factor levels rather than internal system inconsistencies. This suggests that at high ω and $\dot{V}_{\mathrm{Ar}}$ levels, powder feeding may reach an operating limit.

The observed trends are attributable to the mechanisms involved in the feeding system and especially to the pressure losses in the conveyance system. At the suction point, a pressure drop occurs since the powder particles are accelerated by the conveying gas, which overcomes their inertia. The presence of powder particles and frictional forces within the piping system leads to an additional pressure drop, with the magnitude of these drops increasing with the amount of powder entering the flow. Analogously, an increase in $\dot{V}_{\mathrm{Ar}}$ leads to an increase in gas velocity and, consequently, a higher pressure drop due to friction at pipe walls. Furthermore, an increase in powder mixture in the conveyance system, or a higher gas velocity, generates turbulence in the flow, causing more particles to collide with the walls, be retarded, and be accelerated again, thus leading to flow fluctuations and further consequences in pressure loss. Consequently, the pressure drop from the inlet and outlet of the system is significantly influenced by the parameters of the feeding process. The reduction in pressure leads to a substantial decrease in $\dot{m}_{powder}$ as a critical point is attained.

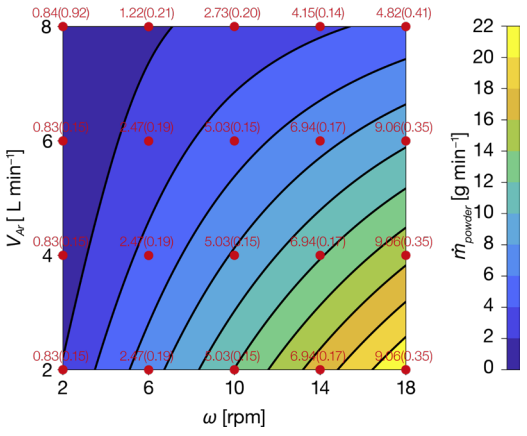


Fig. 6: $\dot{m}_{powder}$ [g min^{-1}] contour plot with the mean(deviation) response.

The regression model for the response surface is developed using stepwise methodology, incorporating linear, quadratic, and interaction terms while excluding uninformative data at $\omega = 22$ rpm. A non-hierarchical approach with a 10 % significance level for entry and removal ensures a conservative model. After four iterations, the model achieves $S = 0.7$, R^2(adj) = 98.7 %, and R^2(pred) = 98.5 %, indicating strong predictive accuracy. Residual analysis confirms normality through the NPP and Anderson-Darling test, with residuals forming a horizontal band around zero, showing no discernible patterns. The final response surface equation (Eq 1) is obtained, with the corresponding plotted response surface shown in Fig. 6, as follows:

$$\dot{m}_{\text{powder}}\ [\text{g min}^{-1}] = 6.574 + 5.911\ \omega - 4.676\ \dot{V}_{\text{Ar}} + 0.794\ \dot{V}_{\text{Ar}}{}^{2} - 3.977\ \omega\ \dot{V}_{\text{Ar}} \quad (1)$$

Although the quadratic term is included in the model, it is found to be less significant, as the non-linearity of the response is better captured by the two-way interaction term.

Conclusions

This study investigated the powder mass flow rate ($\dot{m}_{powder}$) of AISI 316L powder in a horizontal disc-based feeder system, employing a General Full Factorial DoE while accounting for potential noise factors. The objective was to characterize powder transport mechanisms and determine their dependence on disk rotation speed (ω) and carrier gas flow rate ($\dot{V}_{\text{Ar}}$), considering boundary conditions (BCs) as covariates. The findings indicate the presence of specific operational ranges that constrain the effective performance of the system. Especially, rotational speed exceeding 18 rpm adversely affected the efficiency of powder conveyance due to an increase in inertia and friction effects. Furthermore, at high $\dot{V}_{\text{Ar}}$ turbulence is generated into the system, amplifying the inertia effect and causing an additional pressure drop, which negatively affects the powder feeding. Findings suggest that $\dot{V}_{\text{Ar}}$ should be set up at the lowest possible level to ensure the lift force on the powder in the carrier gas is maintained, as well as to shield the melt pool if the same gas is utilised for both purposes. Future studies should refine the $\dot{V}_{\text{cg}}$ range, increase replications, and explore alternative DoE designs to enhance the robustness of the response model and reduce standard error in regression coefficients.

Acknowledgement

This study was carried out within the MICS (Made in Italy – Circular and Sustainable) Extended Partnership and received funding from the European Union Next-GenerationEU (PIANO NAZIONALE DI RIPRESA E RESILIENZA (PNRR) – MISSIONE 4 COMPONENTE 2, INVESTIMENTO 1.3 – D.D. 1551.11-10-2022, PE00000004). This manuscript reflects only the authors' views and opinions, neither the European Union nor the European Commission can be considered responsible for them. This work has been supported by the Interdepartmental Centre for Integrated Additive Manufacturing (IAM@PoliTo) at the Politecnico di Torino, Torino, Italy.

References

[1] ISO/ASTM 52900:2021(E), Additive Manufacturing - General Principles - Fundamentals and vocabulary, American Society for Testing and Materials (ASTM) International, West Conshohocken (USA), 2021.

[2] A.J. Pinkerton, Advances in the modeling of laser direct metal deposition, J. Laser Appl. 27, S15001 (2015) 1-7. https://doi.org/10.2351/1.4815992

[3] M. Ansari, A. Mohamadizadeh, Y. Huang, V. Paserin, E. Toyserkani, Laser directed energy deposition of water-atomized iron powder: Process optimization and microstructure of single-tracks, Opt. Laser Technol. 112 (2019) 485-93. https://doi.org/10.1016/j.optlastec.2018.11.054

[4] M.A. Jackson, A. Kim, J.A. Manders, D.J. Thoma, F.E. Pfefferkorn, Production of mechanically-generated 316L stainless steel feedstock and its performance in directed energy deposition processing as compared to gas-atomized powder, CIRP J. Manuf. Sci. Technol. 31 (2020) 233-43. https://doi.org/10.1016/j.cirpj.2020.05.014

[5] A.B. Spierings, M. Voegtlin, T. Bauer, K. Wegener, Powder flowability characterisation methodology for powder-bed-based metal additive manufacturing, Prog. Addit. Manuf. 1 (2016) 9-20. https://doi.org/10.1007/s40964-015-0001-4

[6] A. Singh, S. Kapil, M. Das, A comprehensive review of the methods and mechanisms for powder feedstock handling in directed energy deposition, Addit. Manuf. 35 (2020) 101388. https://doi.org/10.1016/j.addma.2020.101388

[7] W.J. Oh, W.J. Lee, M.S. Kim, J.B. Jeon, D.S. Shim, Repairing additive-manufactured 316L stainless steel using direct energy deposition, Opt. Laser Technol. 117 (2019) 6-17. https://doi.org/10.1016/j.optlastec.2019.04.012

[8] A.D. Iams, M.Z. Gao, A. Shetty, T.A. Palmer, Influence of particle size on powder rheology and effects on mass flow during directed energy deposition additive manufacturing, Powder Technology. 396 (2022) 316-26. https://doi.org/https://doi.org/10.1016/j.powtec.2021.10.059

[9] L. Simoneau, A. Bois-Brochu, C. Blais, Tensile Properties of Built and Rebuilt/Repaired Specimens of 316L Stainless Steel Using Directed Energy Deposition, J. Mater. Eng. Perform. 29 (2020) 6139-46. https://doi.org/10.1007/s11665-020-05087-z

[10] J. Whiting, A. Springer, F. Sciammarella, Real-time acoustic emission monitoring of powder mass flow rate for directed energy deposition, Addit. Manuf. 23 (2018) 312-8. https://doi.org/https://doi.org/10.1016/j.addma.2018.08.015

[11] A. Aversa, G. Marchese, E. Bassini, Directed energy deposition of aisi 316l stainless steel powder: Effect of process parameters, Metals. 11 (2021) https://doi.org/10.3390/met11060932

[12] P. Mathews, Sample size calculations: Practical methods for engineers and scientists, first ed., Fairport Harbor, Ohio, 2010.

[13] F. Faul, E. Erdfelder, A.G. Lang, A. Buchner, G*Power 3: A flexible statistical power analysis program for the social, behavioral, and biomedical sciences, Behav. Res. Methods. 39 (2007) 175-91. https://doi.org/10.3758/BF03193146